nature geoscience
SUPPLEMENTARY INFORMATION
DOI: 10.1038/NGEO2649

Tohoku rupture reloaded?

Roland Bürgmann[1*], Naoki Uchida[2], Yan Hu[1], and Toru Matsuzawa[2]
[1]Department of Earth and Planetary Science and Berkeley Seismological Laboratory, University of California, Berkeley, California, USA.
[2]Graduate School of Science, Tohoku University, Sendai, Japan.

I. Mechanism type classifications

We used the focal mechanism catalogue of F-net by the National Research Institute for Earth Science and Disaster Prevention[1] to classify faulting types. The catalogue is based on centroid moment tensor determination from broadband seismograms by the method of Dreger and Helmberger[2]. We used the solutions for events with variance reduction of 80% or larger and used three stations to ensure the quality of the mechanisms for the period from January 1998 to May 2015. The faulting types are classified to reverse, normal, strike-slip, and other (or oblique) types based on the method of Frohlich[3] in which plunge angle of P, T and B axis are evaluated.

In Fig. S1 we show the temporal change of the fraction of the four faulting types within the 10m coseismic slip contour of the finite slip model of Yagi and Fukahata[4] which is the same region that Tormann *et al*[5] investigated for temporal change of b-values in their Figure 3a (see Fig. 1f). Earthquakes within 30 km from the plate boundary[6, 7] were used. The fraction estimate was performed for every 30 earthquakes that do not encompass the time of the Tohoku-oki earthquake. The result shows a switch of dominant faulting types from thrusting to normal or other (oblique) type at the time of the Tohoku-oki earthquake[8,9]. Aftershocks primarily occurred in different volumes in both the footwall and hanging wall of the rupture[10] and reverse-faulting events make up only 23 % of the catalogued 2011-2014 focal mechanisms. Changes in the fractions of focal mechanism types during the years following the earthquake are more modest. The mechanisms and locations of the near-field aftershocks do not yet indicate a return to thrust-loading stress conditions on the rupture zone (Fig. 1a-d).

II. Estimation of *b*-values

We use all available earthquakes described above in northeastern Japan (Fig. S2) to plot the frequency distribution of earthquake size based on F-net seismic moment for each faulting

 DOI: 10.1038/NGEO2649

type (Fig. S3). We calculated the *b*-value using a maximum likelihood technique[11,12] and the obtained values are shown in Table S1. We adopted the magnitude of completeness M_c of the catalogue (Mw 4.0)[13] for the estimation but use of a higher completeness magnitude (Mw 4.5) and other area and time span of the analysis also show similar results (Table S1). We also consider focal mechanism catalogs obtained with lower and higher variance-reduction thresholds of 70% and 85%, which also lead to similar results (Table S1 and Fig. S4). Independent of our selection criteria, the frequency distribution of earthquake size show clear dependence on faulting type. Normal faulting and other type earthquakes that are dominant after the Tohoku-oki earthquake in the coseismic slip area have larger *b*-values and reverse faulting earthquakes have a smaller *b*-value, consistent with the *b*-value dependency on mechanism type for other catalogues[14]. Note that the division of the catalogue by focal mechanism type for estimating *b*-values also means selecting different volumes of analysis because each faulting type dominantly occurs in distinct locations (e.g., normal faulting earthquakes within the subducting slab in the outer rise region and in the hanging wall of the high-slip zone).

In Figure 1e of the main text, the temporal change of b-value expected from the mechanism fraction of reverse, normal, strike-slip, and other type earthquakes was calculated as follows

$$b = \sum_{i=1}^{4} w_i b_i$$

, where w_i and b_i are the fraction of the *i*-th mechanism type within the 10 m slip area and *b*-value of *i*-th mechanism type in northeastern Japan, respectively. The time series (Fig. 1e) shows similar coseismic and postseismic temporal changes as the *b*-values shown in Fig. 3a of Tormann *et al*[5] (Fig. 1f), but the amplitude of observed b-value changes are larger than those inferred from the mechanism-type changes alone. The temporal change of the fraction of mechanism type appears to contribute to the coseismic increase and postseismic decay of the inferred *b*-value, although the full explanation of such temporal changes remains for further study.

III. Finite element model of stress evolution

We use the same three-dimensional (3D) viscoelastic finite element model (FEM) as presented in Hu et al.[15] to study the stress evolution of the fault in response to four primary subduction zone processes; (1) the coseismic rupture, (2) the relocking of the fault, (3) viscoelastic relaxation of the upper mantle, and (4) afterslip following the 2011 earthquake.

The FEM includes a 40-km-thick elastic continental lithosphere, an 80-km-thick elastic oceanic lithosphere including the subduction slab, and a viscoelastic continental and oceanic upper mantle. Model boundaries are hundreds of kilometers from the rupture area to eliminate artifacts of boundary effects. Shear moduli of the elastic lithosphere and viscoelastic upper mantle are 48 GPa and 64 GPa, respectively. Poisson's ratio is assumed to be 0.25 in the entire model domain. The bi-viscous Burgers rheology is assumed to represent the viscoelastic upper mantle to capture the observed rapid early relaxation[16]. Steady-state Maxwell viscosities η_M of the continental and oceanic upper mantle are 3×10^{19} Pa s and 10^{20} Pa s, respectively. Afterslip of the fault is modeled through a 2-km-thick weak shear zone at the subduction interface. η_M of the shear zone at depths ≤50 km is 10^{17} Pa s. At greater depths (50 – 100 km), $\eta_M = 5 \times 10^{17}$ Pa s. The transient Kelvin viscosity η_K is assumed to be one order of magnitude lower than that of η_M in all viscoelastic units.

The earthquake is modeled as an instantaneous forward slip of the fault using the split-node method[17]. The average coseismic stress drop in the high-slip zone is about ~10 MPa, consistent with previous estimates[18,19] Relocking of the fault is modeled as slow backward slip of the fault at the subduction rate[20]. The locked region of the fault is enclosed by the 10-meter coseismic slip contour lines[21] (white solid lines in Fig. S5). We applied a uniform subduction rate of 8 cm/yr[22] over the locked region. We also tested 6 cm/yr and 10 cm/yr to study the model sensitivies (grey shaded region in Fig. 1g). Because we focus on the general pattern of the stress evolution, we do not further explore additional heterogeneities of the locked region and subduction rates.

Despite the simplicity of the interseismic model, the model FEM of relocking produces a good fit to the observed interseismic surface velocities (Fig. S5). The model parameters governing afterslip and viscoelastic relaxation provided above are constrained by GPS, seafloor geodetic data and repeating micro-earthquake recurrence intervals[15]. In our calculations of postseismic and interseismic stress changes we average shear stress over a 60 km by 60 km region within the high-slip zone of the Tohoku earthquake (thick black rectangle in Fig. S5).

 DOI: 10.1038/NGEO2649

Table S1. *b* values for each faulting type for northeastern Japan (Fig. S2). A total of 7674 events are considered with a minimum magnitude for the analysis of Mw 4.0 and a variance reduction threshold of ≥ 80 %. The uncertainties shown in parentheses are estimated by the method of Shi and Bolt[23]. Additional columns are the *b*-values calculated for a completeness magnitude of Mw 4.5, for the area outside of the 10 m coseismic slip contour, for the period before the Tohoku-oki earthquake, for the period after the Tohoku-oki earthquake, for the dataset with variance reduction (VR) of ≥85% (5455 events), and for the dataset with variance reduction of ≥70% (11066 events).

Faulting type	b−value	Mc=4.5	outside	before M9	after M9	VR≥85%	VR≥70%
thrust	0.91 (0.02)	0.96 (0.03)	0.91 (0.02)	0.87 (0.02)	0.94 (0.03)	0.90 (0.02)	0.91 (0.02)
strike slip	1.08 (0.09)	1.16 (0.16)	1.21 (0.11)	1.49 (0.17)	0.90 (0.10)	1.16 (0.10)	1.10 (0.08)
normal	1.05 (0.04)	1.06 (0.07)	1.04 (0.05)	0.89 (0.09)	1.05 (0.05)	1.06 (0.05)	1.05 (0.04)
other	1.17 (0.04)	1.19 (0.07)	1.14 (0.04)	1.12 (0.05)	1.19 (0.05)	1.17 (0.04)	1.13 (0.03)

DOI: 10.1038/NGEO2649

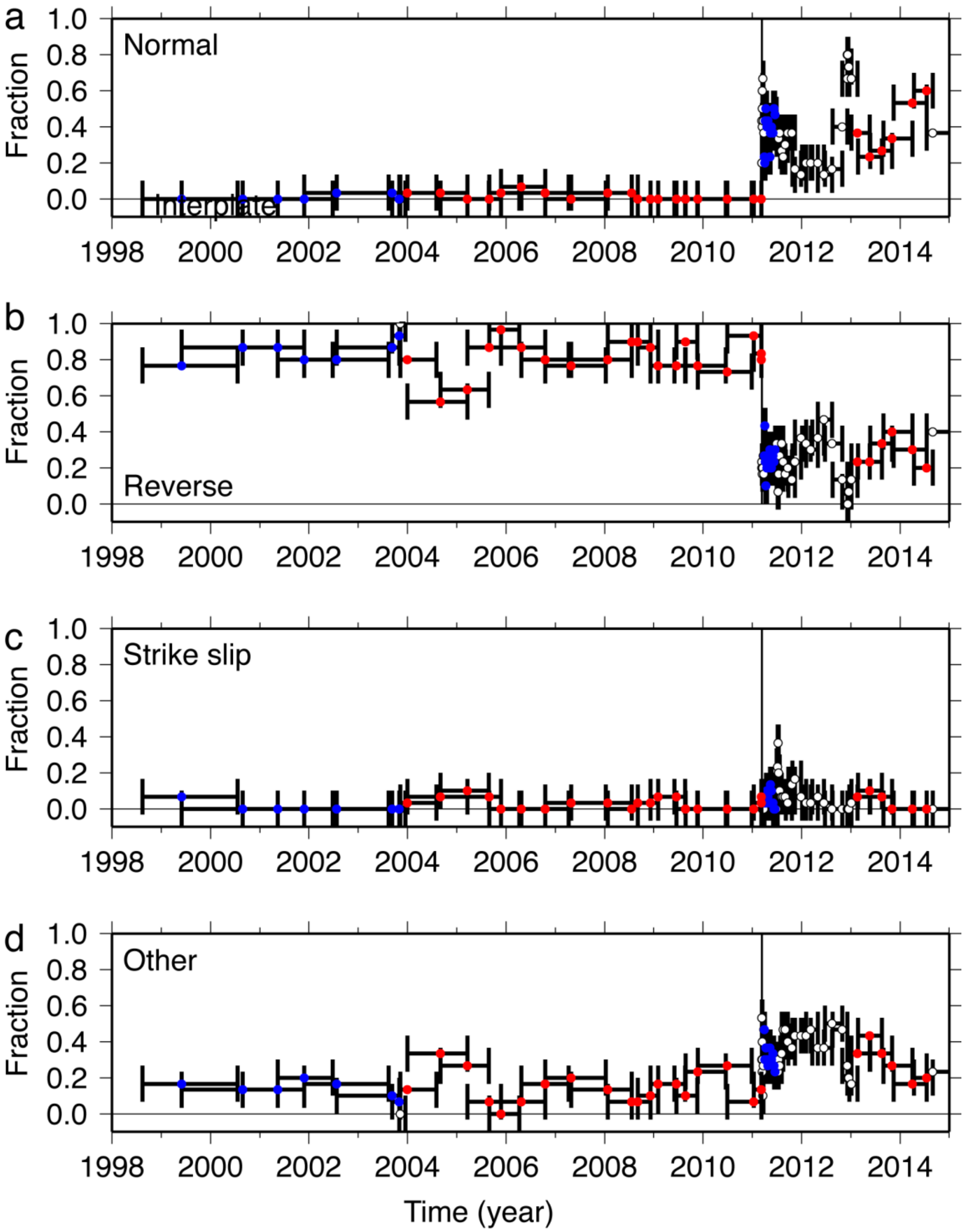

Fig. S1 Fraction of catalogue events of each faulting type as a function of time. (a) Normal-faulting type, (b) reverse-faulting type, (c) strike-slip faulting type, and (d) other faulting type. The window size is 30 earthquakes, overlapping by 15 earthquakes. Vertical line denotes the time of the Tohoku-oki earthquake. Blue and red symbols before the Tohoku-oki earthquake show the periods T1 and T2 defined by Tormann *et al*[5], respectively. Blue and red symbols after the Tohoku-oki earthquake show the periods T3 and T4 defined by Tormann *et al*[5], respectively.

 DOI: 10.1038/NGEO2649

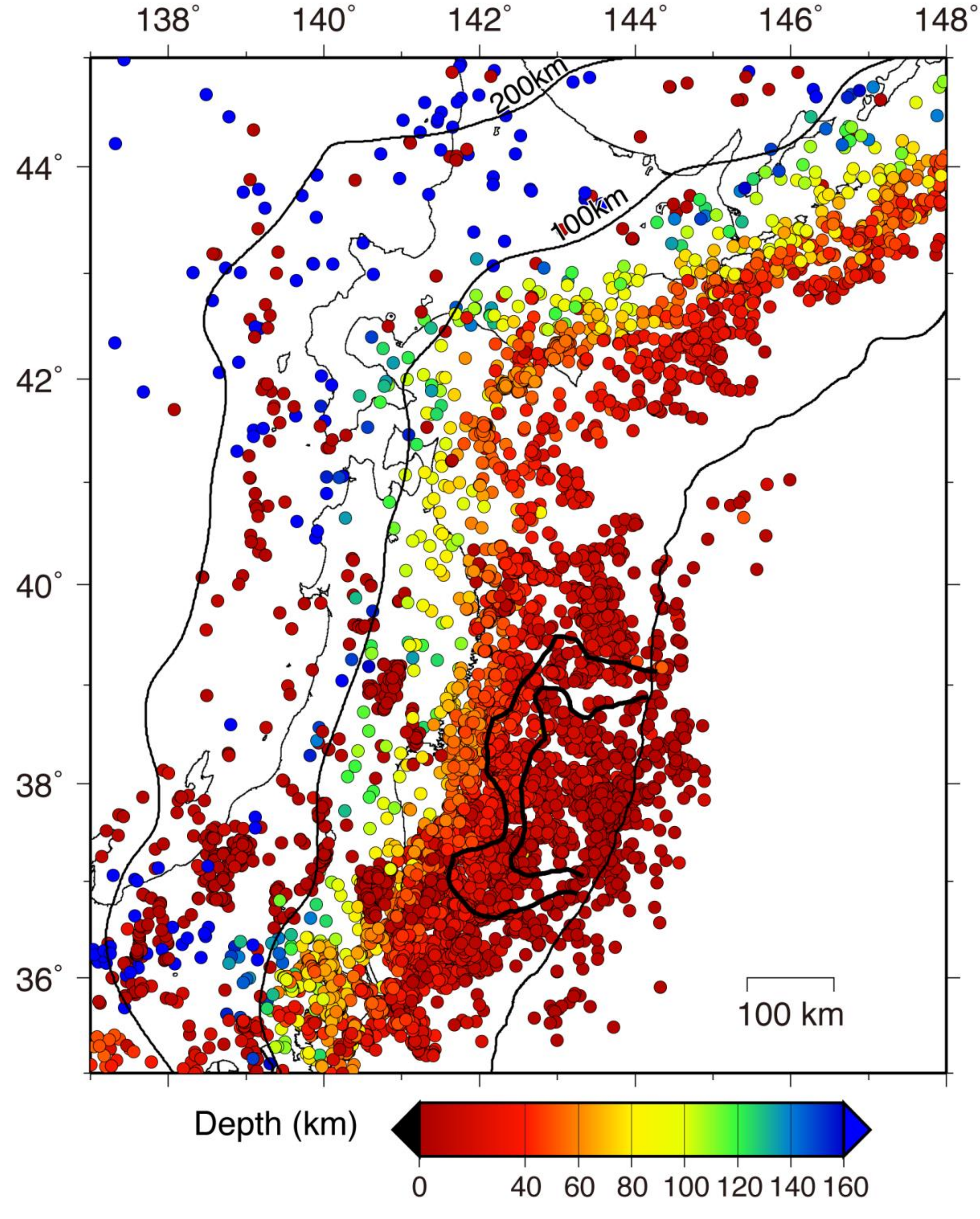

Fig. S2 Distribution of earthquakes used for the *b*-value estimation. Colors show the depth of earthquakes. Thick black contours show 10m and 20m coseismic slip of the Tohoku-oki earthquake[4]. Thin black countours are depth to slab[24].

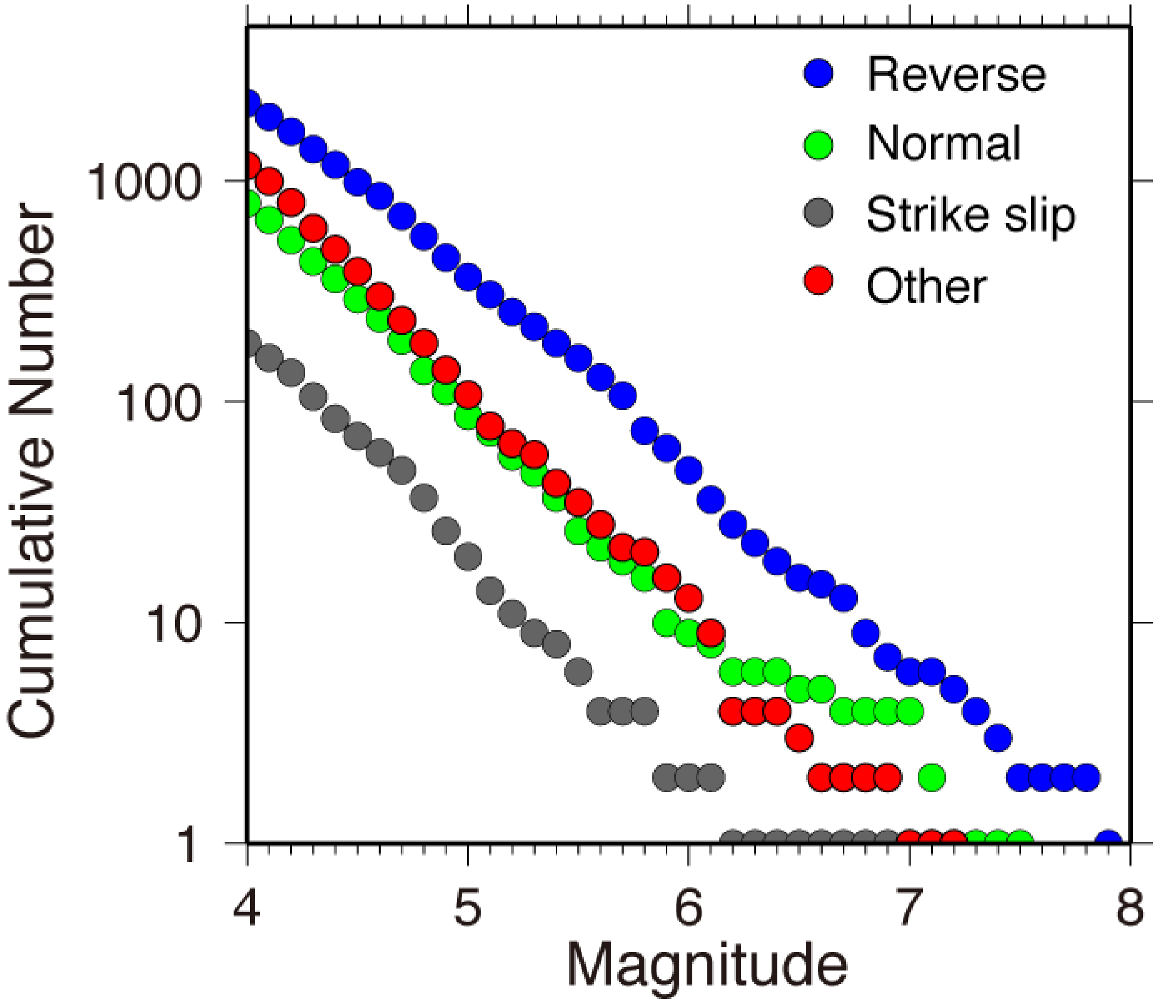

Fig. S3 Frequency distribution of earthquake size for each mechanism type based on F-net seismic moment. The cumulative numbers were calculated for earthquakes shown in Fig. S2.

 DOI: 10.1038/NGEO2649

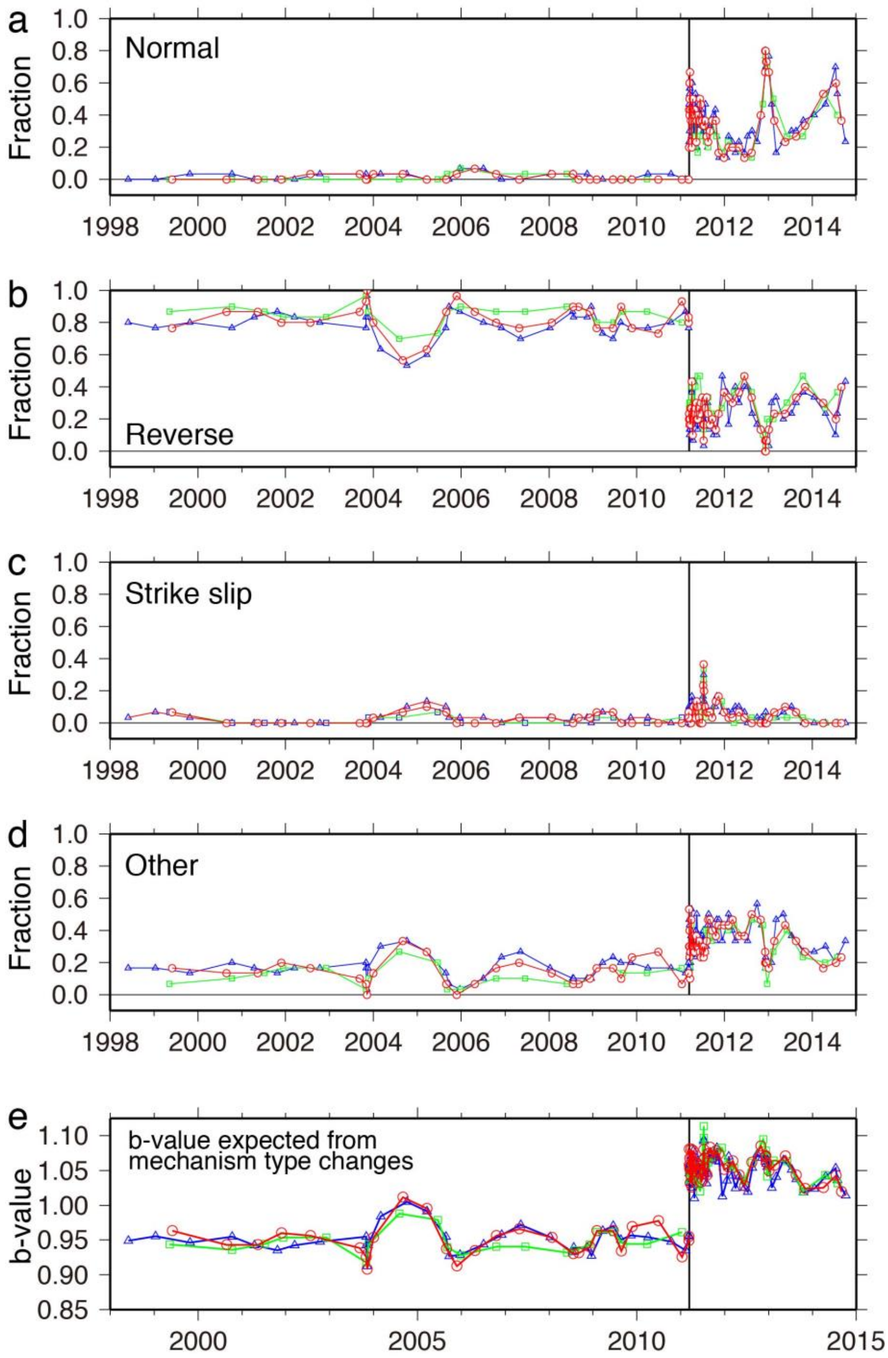

Fig. S4 (a-d) Fraction of catalogue events of each faulting type as a function of time for different variance reduction (VR) thresholds used in the event selection. See Table S1 for the mechanism-dependent *b* values determined for the corresponding event populations in northeastern Japan. Blue line and triangles show the result for VR ≧ 70%. Red line and circles show the result for VR ≧ 80% (same as Fig. S1). Green line and squares show the result for VR ≧ 85%. (e) Time series of b-value within the 10 m slip contour expected from change in distribution of focal mechanisms (a-d) and *b* values determined for each mechanism type (Table S1). Blue, red and green colors show the expected *b* values when VR ≧ 70%, 80% and 85% are used.

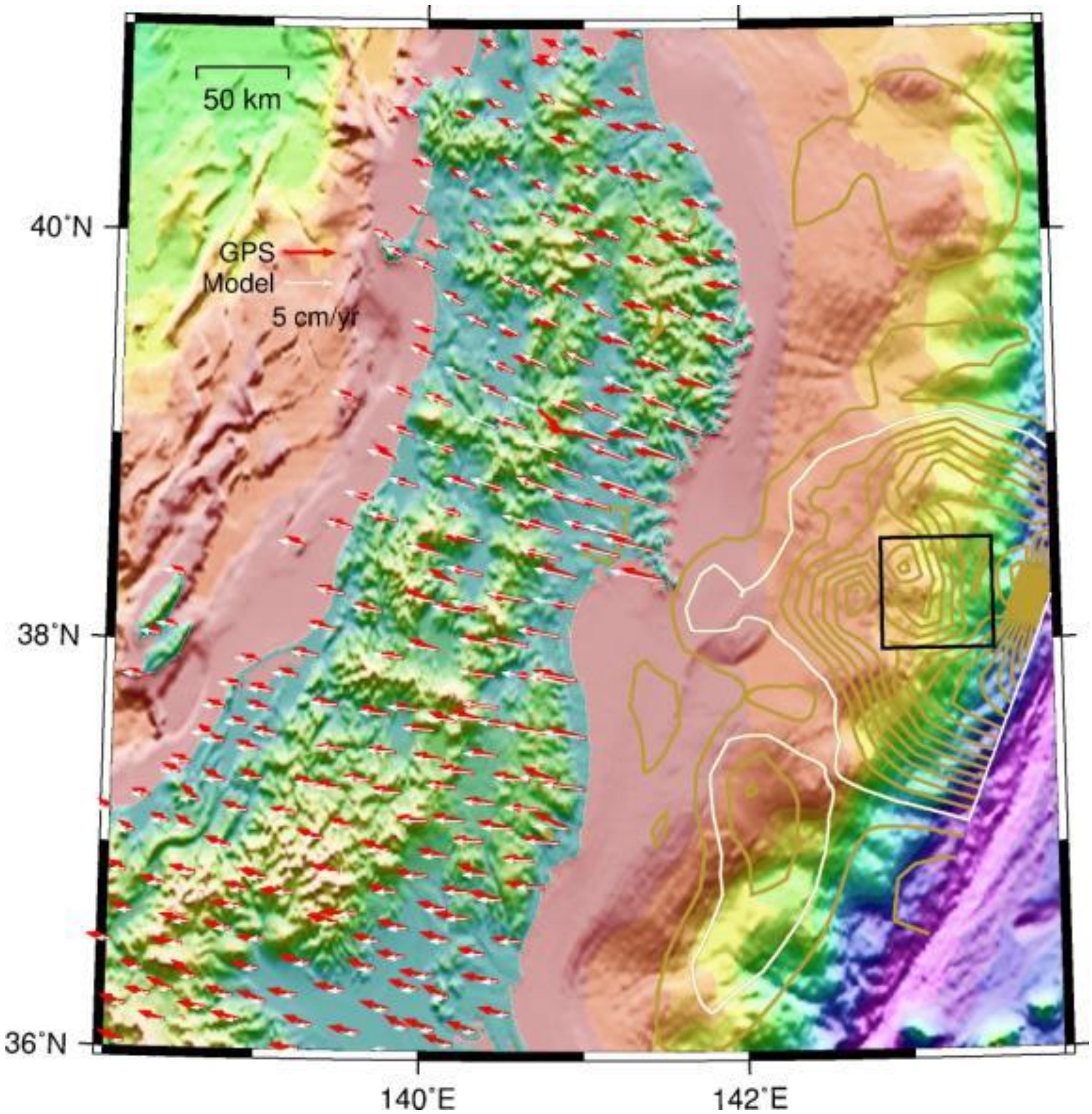

Fig. S5. Interseismic velocities in northeast Japan. Brown lines represent coseismic rupture contours of the 2011 Tohoku earthquake at 5-m intervals[21]. Red arrows represent observed interseismic velocities at GEONET stations[15]. White arrows represent surface velocities predicted by relocking models of locked regions outlined by 10-m (white solid lines) slip contour lines. The subduction rate is assumed to be fixed at 8 cm/yr[22].

DOI: 10.1038/NGEO2649

References

1 Okada, Y. *et al.* Recent progress of seismic observation networks in Japan—Hi-net, F-net, K-NET and KiK-net—. *Earth, Planets and Space* **56**, xv-xxviii (2004).

2 Dreger, D. S. & Helmberger, D. V. Determination of source parameters at regional distances with three-component sparse network data. *Journal of Geophysical Research: Solid Earth* **98**, 8107-8125, doi:10.1029/93JB00023 (1993).

3 Frohlich, C. & Apperson, K. D. Earthquake focal mechanisms, moment tensors, and the consistency of seismic activity near plate boundaries. *Tectonics* **11**, 279-296, doi:10.1029/91TC02888 (1992).

4 Yagi, Y. & Fukahata, Y. Rupture process of the 2011 Tohoku-oki earthquake and absolute elastic strain release. *Geophysical Research Letters* **38**, L19307, doi:10.1029/2011GL048701 (2011).

5 Tormann, T., Enescu, B., Woessner, J. & Wiemer, S. Randomness of megathrust earthquakes implied by rapid stress recovery after the Japan earthquake. *Nature Geosci* **8**, 152-158, doi:10.1038/ngeo2343 http://www.nature.com/ngeo/journal/v8/n2/abs/ngeo2343.html - supplementary-information (2015).

6 Nakajima, J. & Hasegawa, A. Anomalous low-velocity zone and linear alignment of seismicity along it in the subducted Pacific slab beneath Kanto, Japan: Reactivation of subducted fracture zone? Geophys. Res. Lett. **33**, doi:10.1029/2006GL026773 (2006).

7 Kita, S., Okada, T., Hasegawa, A., Nakajima, J. & Matsuzawa, T. Anomalous deepening of a seismic belt in the upper-plane of the double seismic zone in the Pacific slab beneath the Hokkaido corner : Possible evidence for thermal shielding caused by subducted forearc crust materials. Earth Planet. Sci. Lett. **290**, 415-426 (2010).

8 Asano, Y. *et al. Earth Planet. Space* **63**, 669-673, doi:10.5047/eps.2011.06.016 (2011).

9 Uchida, N. & Matsuzawa, T. *Earth Planet. Sci. Lett.* **374**, 81-91, doi:10.1016/j.epsl.2013.05.021 (2013).

10 Obana, K. *et al. Earth Planet. Sci. Lett.* **382**, 111-116, doi:10.1016/j.epsl.2013.09.007 (2013).

11 Aki, K. Maximum Likelihood Estimate of b in the Formula logN= a-bM and its Confidence Limits. *Bull. Earthq. Res. Inst.* **43**, 237-239 (1965).

12 Utsu, T. A method for determining the value of b in a formula log n = a – bM showing the magnitude-frequency relation for earthquakes. *Geophys. Bull. Hokkaido Univ.* **13**,

99-103 (1965).

13 Kato, A. & Igarashi, T. Regional extent of the large coseismic slip zone of the 2011 Mw 9.0 Tohoku-Oki earthquake delineated by on-fault aftershocks. *Geophysical Research Letters* **39**, doi:10.1029/2012gl052220 (2012).

14 Schorlemmer, D., Wiemer, S. & Wyss, M. Variations in earthquake-size distribution across different stress regimes. *Nature* **437**, 539-542 (2005).

15 Hu, Y., Bürgmann, R., Uchida, N., Banerjee, P. & Freymueller, J. T. Stress-driven Relaxation of Heterogeneous Upper Mantle and Time-dependent Afterslip Following the 2011 Tohoku Earthquake. *J. Geophys. Res.* **120**, doi:10.1002:2015JB012508 (2015).

16 Bürgmann, R., & Dresen, G. Rheology of the lower crust and upper mantle: Evidence from rock mechanics, geodesy, and field observations, *Annu. Rev. Earth Planet. Sci.* **36**, 531–567, doi:10.1146/annurev.earth.36.031207.124326 (2008).

17 Melosh, H. J., & Raefsky, A. A simple and efficient method for introducing faults into finite element computations. *Bull. Seismol. Soc. Am.* 71, 1391-1400 (1981).

18 Hasegawa, A., Yoshida, K. & Okada, T. *Earth Planet. Space* **63**, 703-707, doi:10.5047/eps.2011.06.007 (2011).

19 Simons, M. *et al. Science* **332**, 1421-1425 (2011).

20 Hu, Y., Wang, K., He, J., Klotz, J., & Khazaradze, J. Three-dimensional viscoelastic finite element model for post-seismic deformation of the great 1960 Chile earthquake. *J. Geophys. Res.* **109**, B12403, doi:10.1029/2004JB003163 (2004).

21 Iinuma, T., Hino, R., Kido, M., Inazu, D., Osada, Y., Ito, Y., Ohzono, M., Tsushima, T., Suzuki, S., Fujimoto, F., & Miura, S. Coseismic slip distribution of the 2011 off the Pacific Coast of Tohoku Earthquake (M9.0) refined by means of seafloor geodetic data. *J. Geophys. Res.* **117**, B07409, doi:10.1029/2012JB009186 (2012).

22 Altamimi, Z., Métivier, L., & Collilieux, X., ITRF2008 plate motion model. *J. Geophys. Res.* **117**, B07402, doi:10.1029/2011JB008930 (2012).

23 Shi, Y. & Bolt, B. A. The standard error of the magnitude-frequency b value. *B Seismol Soc Am* **72**, 1677-1687 (1982).

24 Hayes, G. P., Wald, D. J. & Johnson, R. L. Slab1.0: A three-dimensional model of global subduction zone geometries. *Journal of Geophysical Research: Solid Earth* **117**, B01302, doi:10.1029/2011JB008524 (2012).